A Saturation Model Based on a Simplified Equivalent Magnetic Circuit for Permanent Magnet Machines

Francesco Lelli[1], Marko Hinkkanen[2], and Fabio Giulii Capponi[1]

[1]Dept. of Astronautical, Electrical and Energy Engineering, Sapienza University of Rome
Rome
[2]Dept. of Electrical Engineering and Automation, Aalto University

April 17, 2024

Abstract

This paper proposes an explicit mathematical model to describe the nonlinear behavior of the permanent magnet synchronous reluctance machine. Although different models for the synchronous reluctance machines are available, extending them to the case of the permanent magnet machine is not trivial due to the effect of the permanent magnets on the rib saturation. This work uses a simplified equivalent magnetic circuit to derive the structure of the proposed model. A nonlinear reluctance is introduced to model the rib saturation. It can be added to the existing model for the synchronous reluctance machine to take into account the effect of the permanent magnets. A simple fitting procedure based on the steepest descent method is proposed to estimate the parameters of the model.

A Saturation Model Based on a Simplified Equivalent Magnetic Circuit for Permanent Magnet Machines

Francesco Lelli
Dept. of Astronautical, Electrical and Energy Engineering
Sapienza University of Rome
Rome, Italy
francesco.lelli@uniroma1.it

Marko Hinkkanen
Dept. of Electrical Engineering and Automation
Aalto University
Espoo, Helsinki
marko.hinkkanen@aalto.fi

Fabio Giulii Capponi
Dept. of Astronautical, Electrical and Energy Engineering
Sapienza University of Rome
Rome, Italy
fabio.giuliicapponi@uniroma1.it

Abstract—This paper proposes an explicit mathematical model to describe the nonlinear behavior of the permanent magnet synchronous reluctance machine. Although different models for the synchronous reluctance machines are available, extending them to the case of the permanent magnet machine is not trivial due to the effect of the permanent magnets on the rib saturation. This work uses a simplified equivalent magnetic circuit to derive the structure of the proposed model. A nonlinear reluctance is introduced to model the rib saturation. It can be added to the existing model for the synchronous reluctance machine to take into account the effect of the permanent magnets. A simple fitting procedure based on the steepest descent method is proposed to estimate the parameters of the model.

Index Terms—Equivalent magnetic circuit, magnetic saturation model, nonlinear fitting, permanent magnet synchronous reluctance machine, steepest descent method.

I. Introduction

The high efficiency and large constant-power speed range capability of permanent magnet synchronous reluctance (PMSyR) machines have earned them attention in the industrial and electric traction fields [1]. Moreover, rare-earth materials are not necessary to build these machines, which makes them a good trade-off between torque density and costs [2]. On the other side, the PMSyR machine shows a complex magnetic model due to the elaborate rotor structure [3] which consequently complicates the control algorithm [4], [5].

An exact model describing the magnetic saturation does not exist but different papers aim to describe this phenomenon for the synchronous reluctance (SyR) machines. The models are composed by one or more self-saturation terms and an additive term that takes into account the cross-saturation phenomenon. If this additive term is defined as it is introduced in [6], the reciprocity condition holds. Good attempts to describe the fluxes-to-currents and currents-to-fluxes relations can be found in [7]–[11]. Regarding the PMSyR machines, their behavior has been analyzed in [12] where a generic formulation is given adapting the analysis in [6]. Because of the permanent magnet (PM) flux linkage, the cross-saturation along the axis with higher reluctance loses the symmetry with respect to the zero current point and a function defined per cases

is necessary to model the cross-saturation contribution for positive and negative current along such axis. However, an explicit mathematical model able to describe the nonlinearities of this machine is not presented in [12].

The PM can be taken into account through a constant current [13] or flux linkage [14] source, according to which of the two quantities is considered as independent variable. At no load, the PM produced flux flows in the ribs and it does not link with the armature windings. On the contrary, when the ribs are saturated by the stator flux, the PM flux concatenating with the windings increases. This phenomenon strongly complicates the magnetic behaviour and the models in the literature are not enough to correctly describe it.

An interesting way to model the magnetic behavior of machines with the PM is presented in [3] for an interior permanent magnet (IPM) machine. The authors use a lumped-parameter model to build an equivalent magnetic circuit in which the rotor geometry is characterized by constant and varying reluctances modeling the flux barriers and the iron core saturation, respectively, and constant flux sources to reproduce the PM flux and the rib saturation. The equivalent circuit approach is based on the geometry of the machine and the flux paths inside it, which makes it particularly appealing to model the rib saturation. In the case of IPM machine, the flux produced by the magnets is strong enough to saturate the ribs for all the operating current points; the same is not true for a PMSyR machine which presents a lower amount of the PM. Relaxing the assumption of the ribs always saturated, a model similar to the one in [3] can be suitable to describe the magnetic saturation for a PMSyR machine.

Another important aspect that must be taken into consideration when dealing with a nonlinear model is the identification procedure. Once the model equation has been defined it is necessary to estimate its parameters. This can be easily done for the parameters appearing linearly through the linear least square (LLS) method but it can be very challenging in case of parameters appearing nonlinearly. Nonlinear optimal problems may converge to a solution that is only locally optimum which strongly depends on the initial conditions.
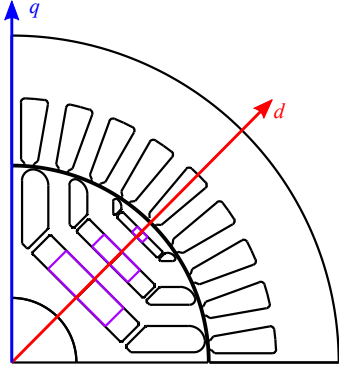
Fig. 1: Rotor pole geometry of a PMSyR machine.

Fig. 2: Simplified equivalent magnetic circuit in the case of a single pole single PM barrier.

In this work, an equivalent circuit for a PMSyR machine with a simple rotor geometry is drawn and solved to shape the current equations as functions of the fluxes in the dq synchronous reference frame:

$$\begin{cases} i_d = i_d\left(\psi_d, \psi_q\right) \\ i_q = i_q\left(\psi_d, \psi_q\right) \end{cases} \tag{1}$$

where ψ_d, ψ_q, i_d, and i_q are the flux linkages and currents along the d and q-axis respectively.

Subsequently, an algorithm based on the LLS method and on the steepest descent method is proposed to estimate the model parameters. One pole of a PMSyR machine is drawn in Fig. 1. The reference axes are chosen with the d-axis along the PM flux direction and the q-axis 90 degrees ahead as it is usual for the PM synchronous machines.

II. SATURATION MODEL

A. Equivalent Circuit

The approach of the equivalent circuit in [3] is used in this section to derive a structure for the proposed model. Fig. 2 shows the single pole equivalent circuit where the stator teeth have been neglected, only one pair of PM barriers is considered for the sake of simplicity. Moreover, single turn windings are considered so that magnetic and electrical quantities coincide.

The red and blue circuits model the d and q-axis magnetic paths, respectively. The air-gap reluctances are modeled as constant terms a_{gd} and a_{gq} while the magnetic behavior of the iron is taken into account by the nonlinear reluctances a_{cd} and a_{cq}. The magnets are modeled using the Norton equivalent circuit as a constant flux source ψ_f and a parallel linear reluctance a_m which models the reluctance of the PM. In parallel to it is added a nonlinear reluctance a_{bd} that models the ribs saturation.

At no load condition, the reluctance a_{bd} allows some part of the flux ψ_f to bypass the air-gap as shown in Fig. 3(a). When a positive current i_d is applied, the flux produced by this current goes through a_{bd} desaturating the ribs. As the amplitude of i_d increases, the flux through a_{bd} decreases until it changes direction [Fig. 3(b)] and the ribs become saturated again for high value of i_d [Fig. 3(c)]. In case of a negative i_d current, the produced flux strengthens the ribs saturation as
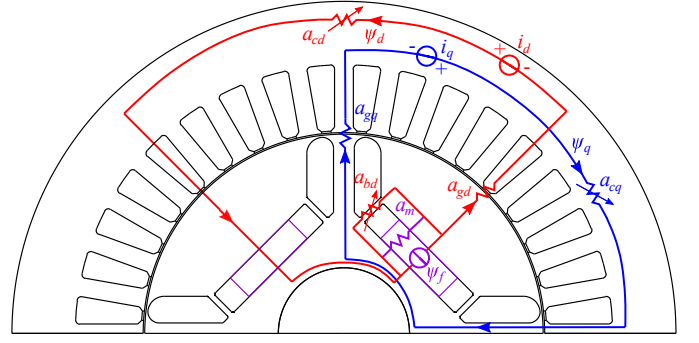
illustrated in Fig. 3(d) where $i_d = -i_n$ is supplied, being i_n the nominal current.

Solving the circuits, the current equations are

$$\begin{aligned} i_d\left(\psi_d, \psi_q\right) &= \left[a_{gd} + a_{cd}\left(\psi_d, \psi_q\right)\right]\psi_d \\ &\quad + \frac{a_m a_{bd}\left(\psi_b, \psi_q\right)}{a_m + a_{bd}\left(\psi_b, \psi_q\right)}\left(\psi_d - \psi_f\right) \\ i_q\left(\psi_d, \psi_q\right) &= \left[a_{gq} + a_{cq}\left(\psi_d, \psi_q\right)\right]\psi_q \\ &\quad + \frac{a_m a_{bq}\left(\psi_b, \psi_q\right)}{a_m + a_{bq}\left(\psi_b, \psi_q\right)}\psi_q \end{aligned} \tag{2}$$

where $\psi_b = \psi_d - \psi_f$ is the flux going through the ribs.

The third term in the $i_d\left(\psi_d, \psi_q\right)$ takes into account the magnets and the rib effects. It is worth noticing that this term must contribute to both d-axis self and cross-saturations and, assuming a_m, a_{bd} positive, when $\psi_d = 0$, i_d is negative and it represents the amplitude of the PM flux equivalent magneto-motive force generating current. Furthermore, notice that the third term in the q-axis model has been added to be able to meet the reciprocity condition. This term can be thought of as the cross-saturation effect the rib nonlinearities have on the q-axis current; if the q-axis flux is null this contribution disappears.

B. Rib Model

The SyR model from [8] is used to describe the main effects of self and cross-saturation of the machine described by the terms a_{gd}, a_{gq}, a_{cd}, and a_{cq} in (2)

$$\begin{aligned} \widetilde{i}_d &= \left(a_{gd} + a_{dd}\left|\psi_d\right|^X + \frac{a_{dq}}{W+2}\left|\psi_d\right|^U\left|\psi_q\right|^{W+2}\right)\psi_d \\ \widetilde{i}_q &= \left(a_{gq} + a_{qq}\left|\psi_q\right|^Y + \frac{a_{dq}}{U+2}\left|\psi_d\right|^{U+2}\left|\psi_q\right|^W\right)\psi_q \end{aligned} \tag{3}$$

The last terms in (2), modeling the rib saturation and PM effects, can be written as

$$\begin{aligned} \frac{a_m a_{bd}\left(\psi_b, \psi_q\right)}{a_m + a_{bd}\left(\psi_b, \psi_q\right)}\psi_b &= g\left(f\left(\psi_b, \psi_q\right)\right)\frac{\partial f\left(\psi_b, \psi_q\right)}{\partial \psi_d} \\ \frac{a_m a_{bq}\left(\psi_b, \psi_q\right)}{a_m + a_{bq}\left(\psi_b, \psi_q\right)}\psi_q &= g\left(f\left(\psi_b, \psi_q\right)\right)\frac{\partial f\left(\psi_b, \psi_q\right)}{\partial \psi_q} \end{aligned} \tag{4}$$

Notice that the reciprocity condition holds for any function g and f used. It can be proved by comparing the partial derivatives of (4).
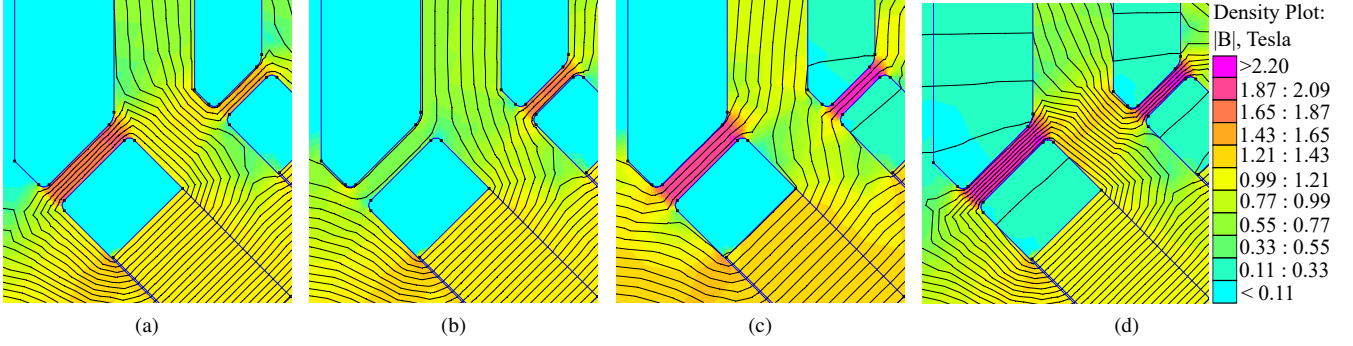
Fig. 3: Rib saturation for $i_q = 0$ A and: (a) $i_d = 0$ A; (b) $i_d = 0.25 i_n$; (c) $i_d = i_n$; (d) $i_d = -i_n$.

If the function $g\left(f\left(\psi_b, \psi_q\right)\right)$ is used to describe the rational structure, the partial derivatives of f are $\partial f / \partial \psi_d = \psi_b$ and $\partial f / \partial \psi_q = \psi_q$. This imposes that the function f is fixed to the form

$$f\left(\psi_b, \psi_q\right) = k_d \psi_b^2 + k_q \psi_q^2 \tag{5}$$

By taking the square root of this term, the result is a weighted module of the flux vector. According to this, and remembering that $g\left(f\left(\psi_b, \psi_q\right)\right)$ has the rational structure in (4), the function g is chosen as

$$g\left(f\left(\psi_b, \psi_q\right)\right) = \frac{a_b \sqrt{\psi_b^2 + k_q \psi_q^2}^T}{1 + \overline{a_b} \sqrt{\psi_b^2 + k_q \psi_q^2}^T} \tag{6}$$

where the coefficient k_d is set to 1 to avoid parameters redundancy. The constant term a_m is collected to common factor and $\overline{a}_b = a_b / a_m$. These choices reduce the number of parameters to tune during the fitting procedure. The entire equations become

$$
\begin{aligned}
i_d &= \widetilde{i}_d + \frac{a_b \overline{\psi}_b^T}{1 + \overline{a}_b \overline{\psi}_b^T} \psi_b \\
i_q &= \widetilde{i}_q + k_q \frac{a_b \overline{\psi}_b^T}{1 + \overline{a}_b \overline{\psi}_b^T} \psi_q
\end{aligned} \tag{7}
$$

where $\overline{\psi}_b = \sqrt{\psi_b^2 + k_q \psi_q^2}$.

As mentioned in Section II-A, the rib term in i_d definition affects both self and cross-saturation, while the last term in i_q affects only the cross-saturation.

It is worth pointing out that (7) are able to describe all the synchronous machines. For an IPM machine, it is expected ψ_f to be high enough to always ensure that the ribs are saturated by the PM flux. In the case of a SyR machine the rib term can be neglected or ψ_f can be set to zero, modeling the rib saturation without the effect of the PM.

The parameters appearing linearly in (7) and (3) can be rewritten collecting a_{gd} and a_{gq}. The equations rearranged in this way are written in (8), where the parameters are defined as: $L_{d0} = a_{gd}^{-1}$, $L_{q0} = a_{gq}^{-1}$, $b_d^X = \frac{a_{gd}}{a_d}$, $b_q^Y = \frac{a_{gq}}{a_q}$, $b_{dd}^{U+W+2} = \frac{a_{dq}}{a_{gd}}$, $b_{qq}^{U+W+2} = \frac{a_{dq}}{a_{gq}}$, $b_{bd}^T = \frac{a_{gd}}{a_b}$, $b_{bq}^T = \frac{a_{gq}}{a_b}$ and $\overline{b}_b^T = \frac{a_{gd}}{\overline{a}_b}$.

With this manipulation, the values L_{d0} and L_{q0} are the unsaturated inductances while the b coefficients are fluxes. All the remaining parameters are pure numbers.

III. FITTING PROCEDURE

The parameter identification procedure has a key role in the definition of a new model. The more the parameters the heavier the estimation is from a computational point of view and the presence of parameters appearing nonlinearly remarkably complicates the problem. For ease of reading, in this section it is referred to parameters that appear linearly and nonlinearly in the model as *linear* and *nonlinear* parameters respectively.

A. Problem Statement

Consider α^l and α^{nl} the set of linear and nonlinear parameters respectively and let $i_d^n\left(\psi_d^n, \psi_q^n\right)$, $i_q^n\left(\psi_d^n, \psi_q^n\right)$ be the nth currents measurements for given fluxes with $\widehat{i}_d^n\left(\psi_d^n, \psi_q^n, \alpha^l, \alpha^{nl}\right), \widehat{i}_q^n\left(\psi_d^n, \psi_q^n, \alpha^l, \alpha^{nl}\right)$ their estimate. The goal of the fitting is to find the set of linear and nonlinear parameters that minimizes the rms of residuals

$$e_{rms}(\alpha^l, \alpha^{nl}) = \sqrt{\frac{1}{N} \sum_{n=1}^{N} e_n^2(\alpha^l, \alpha^{nl})} \tag{9}$$

where $e_n(\alpha^l, \alpha^{nl}) = i^n - \widehat{i}^n(\alpha^l, \alpha^{nl})$ is the residual of the nth sample and N is the number of samples. The dependency of the residuals and their rms value from the current ad flux measurements have been dropped for the sake of simplicity.

B. Proposed Fitting Method

To solve the parameter identification, the fitting problem has been split into two smaller problems that are iteratively solved. At each iteration, the algorithm searches for a better guess of the nonlinear parameters α^{nl} with a procedure inspired by the steepest descent method. Subsequently, fixed α^{nl}, the linear parameters α^l are estimated using the LLS method.

The descent methods are a family of algorithms to iteratively find a local minimum for the cost function (in this work e_{rms}) enforcing the descending condition

$$e_{rms}(\alpha_{k+1}^l, \alpha_{k+1}^{nl}) < e_{rms}(\alpha_k^l, \alpha_k^{nl}) \tag{10}$$

$$i_d = \frac{\psi_d}{L_{d0}} \left[1 + \left(\frac{|\psi_d|}{b_d} \right)^X + \frac{1}{W+2} \frac{|\psi_d|^U |\psi_q|^{W+2}}{b_{dd}^{U+W+2}} \right] + 2 \frac{\psi_b}{L_{d0}} \left(\frac{|\overline{\psi}_b|}{b_{bq}} \right)^T \left[1 + \left(\frac{|\overline{\psi}_b|}{\overline{b}_b} \right)^T \right]^{-1}$$

$$i_q = \frac{\psi_q}{L_{q0}} \left[1 + \left(\frac{|\psi_q|}{b_q} \right)^Y + \frac{1}{U+2} \frac{|\psi_d|^{U+2} |\psi_q|^W}{b_{qq}^{U+W+2}} \right] + 2 \frac{k_q \psi_q}{L_{q0}} \left(\frac{|\overline{\psi}_b|}{b_{bq}} \right)^T \left[1 + \left(\frac{|\overline{\psi}_b|}{\overline{b}_b} \right)^T \right]^{-1}$$

(8)

where k is the current iteration. Each iteration consists of two steps:

1) find the descent direction vector h;
2) find the step length δ to move along h.

The steepest descent method involves the definition of h as the direction that provides the best improvement in the cost function and it is computed as $h = -de_{rms}(\alpha^l, \alpha^{nl})/d(\alpha^l, \alpha^{nl})$. However, since e_{rms} is a complicated function, computing its derivative can be tedious, so the step length δ is chosen a priori, and the vector h is chosen according to the discrete derivative of e_{rms}.

The entire algorithm is summarized as follows, where P is the number of nonlinear parameters to estimate:

1) Set the initial guess for the nonlinear parameters $\widehat{\alpha}^{nl} = \left[\widehat{\alpha}_1^{nl}, ..., \widehat{\alpha}_P^{nl} \right] = [k_{b0}, \overline{a}_{b0}, X_0, Y_0, U_0, W_0, T_0, \psi_{f0}]$ and the respective discrete variations $\delta \alpha^{nl} = \left[\delta \alpha_1^{nl}, ..., \delta \alpha_P^{nl} \right]$.
2) Use the LLS method to compute the optimal linear parameters $\widehat{\alpha}^l$ according to the fixed nonlinear parameters $\widehat{\alpha}^{nl}$ and evaluate $e_{rms} \left(\widehat{\alpha}^l, \widehat{\alpha}^{nl} \right)$ as in (9).
3) Increase and decrease the mth component of the vector $\widehat{\alpha}^{nl}$ by $\delta \alpha_m^{nl}$:

$$\widehat{\alpha}^{nl+} = \widehat{\alpha}^{nl} + \mathbf{1} \delta \alpha_m^{nl}$$
$$\widehat{\alpha}^{nl-} = \widehat{\alpha}^{nl} - \mathbf{1} \delta \alpha_m^{nl}$$

(11)

where $\mathbf{1}$ is a vector of dimension P of zeros except for the mth components that is set to 1. For both the increment and decrement, solve the LLS problem to compute the optimal linear parameters $\widehat{\alpha}^l$, compute the new value of e_{rms} and its forward and backward discrete derivatives with respect to the component of $\widehat{\alpha}_m^{nl}$:

$$\frac{\partial^+ e_{rms}}{\partial^+ \alpha_m^{nl}} = \frac{e_{rms} \left(\alpha^l, \widehat{\alpha}^{nl+} \right) - e_{rms} \left(\alpha^l, \widehat{\alpha}^{nl} \right)}{\delta \alpha_m^{nl}}$$

(12)

$$\frac{\partial^- e_{rms}}{\partial^- \alpha_m^{nl}} = \frac{e_{rms} \left(\alpha^l, \widehat{\alpha}^{nl-} \right) - e_{rms} \left(\alpha^l, \widehat{\alpha}^{nl} \right)}{\delta \alpha_m^{nl}}$$

(13)

4) Among the parameters that have at least one of the derivatives negative, choose the one with the highest absolute value of $\frac{\partial^\pm e_{rms}}{\partial^\pm \alpha^{nl}}$.
5) Modify the selected nonlinear parameter as:

$$\begin{cases} \widehat{\alpha}^{nl} = \widehat{\alpha}^{nl} + \mathbf{1} \delta \alpha^{nl} & \text{if} \quad \partial^+ < 0 \\ \widehat{\alpha}^{nl} = \widehat{\alpha}^{nl} - \mathbf{1} \delta \alpha^{nl} & \text{if} \quad \partial^- < 0 \end{cases}$$

(14)

and compute the relative linear parameters using the LLS method.

TABLE I: Nonlinear parameters initial guess.

X	Y	U	W	T	k_q	ψ_f	$\overline{a}_b$
4	5	4	4	2	1	0.066	1

TABLE II: Nonlinear parameters discrete increment definition.

δX	δY	δU	δW	δT	δk_q	$\delta \psi_f$	$\delta \overline{a}_b$
1	1	1	1	1	0.01	0.001	1

6) Repeat from step 3) until there are no parameters with a negative derivative. If step 4) fails to find a parameter with a negative derivative, the local optimal solution is the one found in the previous iteration.

This algorithm gives a systematic way to compute the nonlinear parameters of the regression problem. Selecting the component of α^{nl} to modify according to the negative derivative of e_{rms} assures the descending condition in (10) and the convergence of the solution to a minimum.

Since only one parameter at a time is modified, at any iteration it is necessary to solve $2P$ LLS problems. If any direction h is admitted once δ is fixed, the number of LLS problems that should be solved would be $3^P - 1$. Notice also that in step 3), it is necessary to compute both the forward and backward derivatives since they can be different due to the discrete nature of the algorithm.

IV. SIMULATIONS

In this section, the analysis is validated through simulations on the machine (Fig. 1) from the SyR-e open-source project [15]. In the test dataset the d and q-axis current are limited within plus and minus twice the nominal current $i_n = 22$ A.

A. State of the Art Model

To highlight the model improvement due to the rib saturation, the model in (7) is compared with

$$i_d = \widetilde{i}_d - i_f$$
$$i_q = \widetilde{i}_q$$

(15)

from [13], where the PMs are modeled by a constant current source i_f and the rib saturation is not modeled.

The parameters of the model (15) are estimated with the procedure introduced in Section III. Fig. 4(a) and (b) show the currents i_d and i_q estimated when the fluxes along q and d-axis respectively are kept constant. Looking at Fig. 4(b) it can be seen that the model can describe the saturation along the q-axis since it is not strongly affected by the rib saturation. On the other hand, looking at Fig. 4(a) it is evident that

TABLE III: Model (7) parameters estimated using the proposed algorithm.

X	Y	U	W	T	k_q	ψ_f	$\bar{b}_b$	L_{d0}	L_{q0}	b_d	b_q	b_{dd}	b_{qq}	b_{bd}	b_{bq}
4	6	2	3	2	0.20	0.162	0.7071	0.0286	0.0422	0.1457	0.1986	0.1336	0.1264	0.0857	0.0706
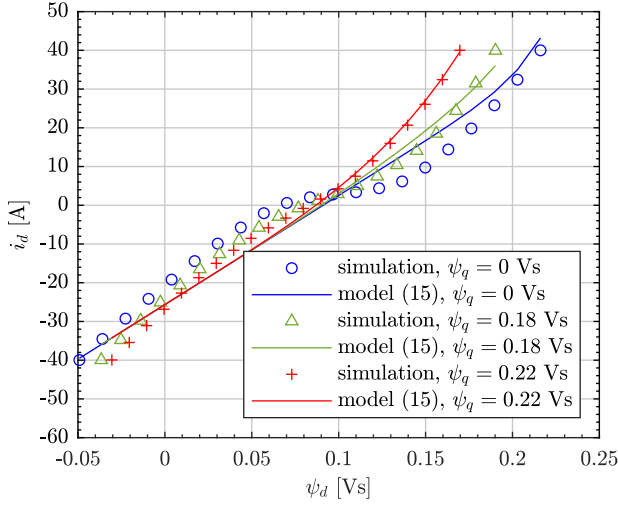
(a)
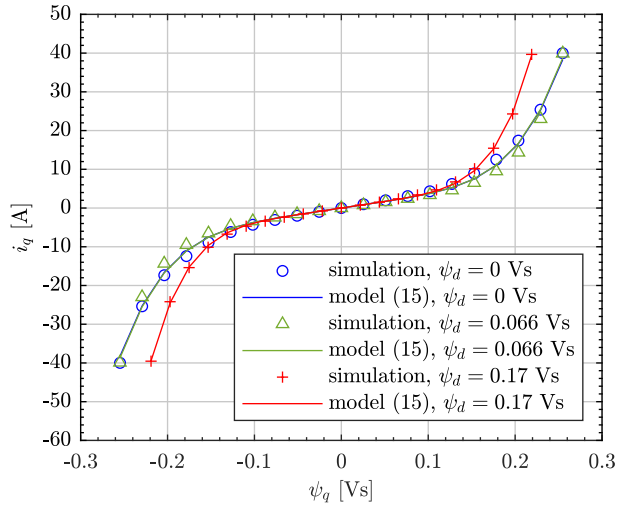
(b)

Fig. 4: Fluxes to currents maps (a) $i_d(\psi_d, \psi_q)$; (b) $i_q(\psi_d, \psi_q)$. With markers the dataset points from simulations, with solid lines the currents estimated with the model in (15).

the nonlinearity along d-axis is not well described and the predicted curves are very close to straight lines.

B. Proposed Model

The initial guess for the parameters appearing nonlinearly is given in Table I and the discrete increments $\delta\alpha^{nl}$ in Table II. The exponents have been restricted to integer numbers, hence their increment is set to 1. The parameter k_q is initialized to 1 so that the vector magnitude definition results as base for the exponential terms. The flux ψ_f is chosen as the no-load PM flux linkage and $\bar{a}_b = 1$. The model is fitted using the algorithm described in Section III-B and the estimated parameters are given in Table III.
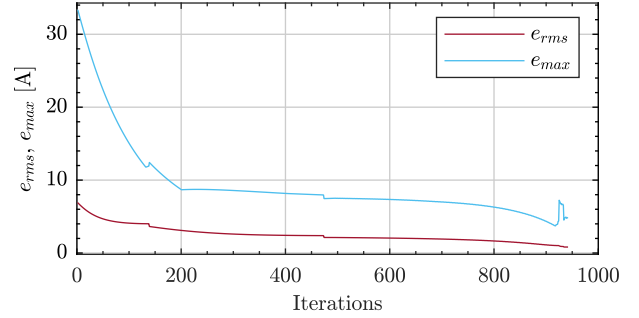

Fig. 5: The rms and maximum residual evolution during the fitting process of model (7).

Fig. 5 shows the evolution of the rms and maximum of the residual evolutions over the iteration process. The e_{rms} is always decreasing because of the descent condition in (10), while the maximum residual can increase because it is not taken into account in the fitting algorithm. However, reducing the average error among the surfaces also implies a remarkable reduction of the maximum error with respect to the initial guess if the number of iterations performed is sufficiently high.

The e_{rms} of the fitted model is 3.73% with respect to the nominal current, while the maximum error e_{max} is 22.17%. Fig. 6(a) and (b) show the match between the dataset points and the estimated surfaces for $i_d(\psi_d, \psi_q)$ and $i_q(\psi_d, \psi_q)$ respectively. Moreover, the larger error is obtained in the i_d map in Fig. 6(a) for the positive values of i_d which are not part of the maximum torque per ampere region of the machine. To better show the goodness of the proposed model, Fig. 7 reports some curves for the estimated i_d and i_q when the flux along the opposite axis is kept constant. Comparing these curves with those estimated with the model (15) in Fig. 4, it is evident the improvement achieved because of the rib saturation model concerning the d-axis saturation.

V. CONCLUSIONS

An explicit mathematical model has been proposed to model the rib saturation in synchronous machines using an equivalent circuit approach. It has been provided a more general formulation for the cross-saturation term that extends the one in the literature. The rib term can be added to the existing SyR machine models to extend them to the case of PMSyR machines.

The fitting procedure for the estimation of the parameters has been investigated due to its importance in the identification of the coefficients appearing nonlinearly. An algorithm based on the steepest descent method was proposed which achieved good performance.
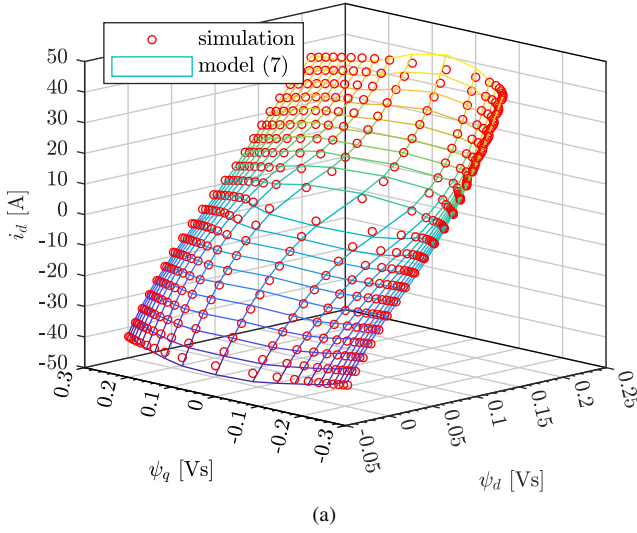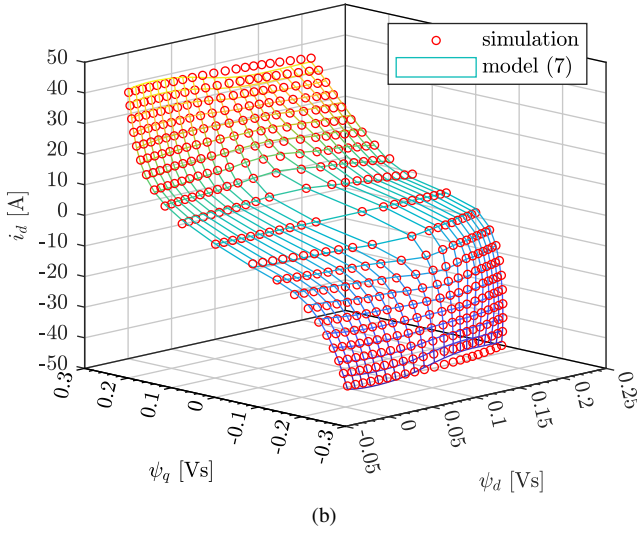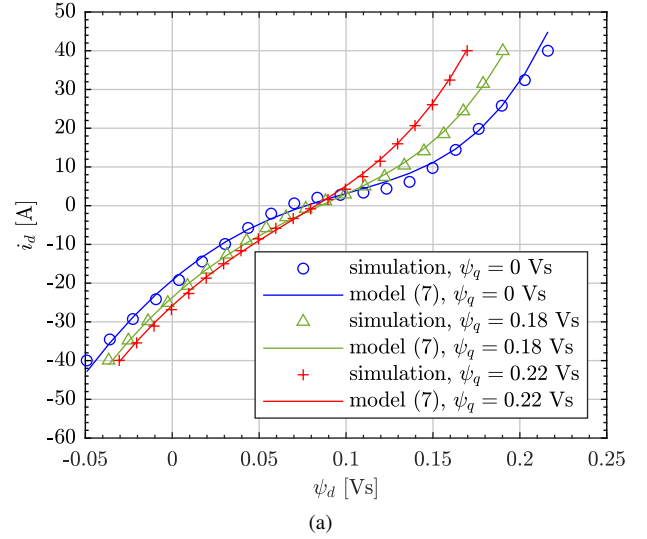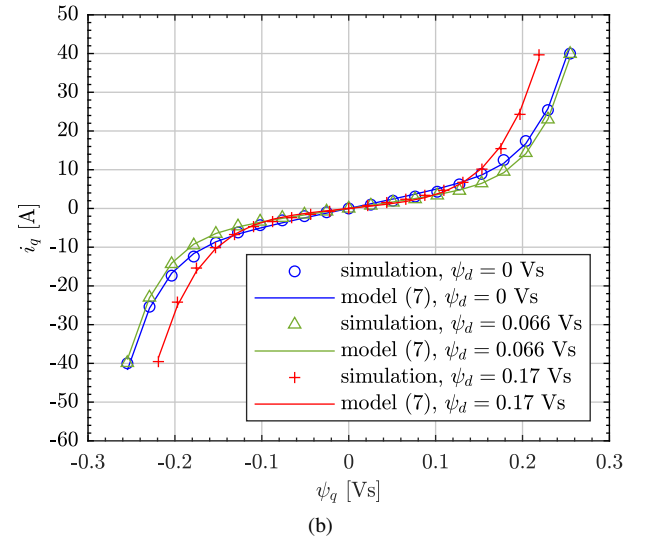
Fig. 6: Fluxes to currents maps (a) $i_d\,(\psi_d, \psi_q)$; (b) $i_q\,(\psi_d, \psi_q)$. With markers the dataset points from simulations, with surfaces the currents estimated with the model (7).

Fig. 7: Fluxes to currents maps (a) $i_d\,(\psi_d, \psi_q)$; (b) $i_q\,(\psi_d, \psi_q)$. With markers the dataset points from simulations, with solid lines the currents estimated with the model in (7).

REFERENCES

[1] M. Murataliyev, M. Degano, M. Di Nardo, N. Bianchi, and C. Gerada, "Synchronous reluctance machines: A comprehensive review and technology comparison," *Proceedings of the IEEE*, vol. 110, no. 3, pp. 382–399, 2022.

[2] G. Pellegrino, T. M. Jahns, N. Bianchi, W. Soong, F. Cupertino, and T. M. Jahns, "Overview of PM/reluctance synchronous machine opportunities and challenges," *The Rediscovery of Synchronous Reluctance and Ferrite Permanent Magnet Motors: Tutorial Course Notes*, pp. 1–26, 2016.

[3] E. C. Lovelace, T. M. Jahns, and J. H. Lang, "A saturating lumped-parameter model for an interior PM synchronous machine," *IEEE Transactions on Industry Applications*, vol. 38, no. 3, pp. 645–650, 2002.

[4] H. A. A. Awan, S. E. Saarakkala, and M. Hinkkanen, "Flux-linkage-based current control of saturated synchronous motors," *IEEE Transactions on Industry Applications*, vol. 55, no. 5, pp. 4762–4769, 2019.

[5] S.-W. Su, H. Börngen, C. M. Hackl, and R. Kennel, "Nonlinear current control of reluctance synchronous machines with analytical flux linkage prototype functions," *IEEE Open Journal of the Industrial Electronics Society*, vol. 3, pp. 582–593, 2022.

[6] A. Vagati, M. Pastorelli, F. Scapino, and G. Franceschini, "Impact of cross saturation in synchronous reluctance motors of the transverse-laminated type," *IEEE Transactions on Industry Applications*, vol. 36, no. 4, pp. 1039–1046, 2000.

[7] T.-G. Woo, S.-W. Park, S.-C. Choi, H.-J. Lee, and Y.-D. Yoon, "Flux saturation model including cross saturation for synchronous reluctance machines and its identification method at standstill," *IEEE Transactions on Industrial Electronics*, vol. 70, no. 3, pp. 2318–2328, 2022.

[8] Z. Qu, T. Tuovinen, and M. Hinkkanen, "Inclusion of magnetic saturation in dynamic models of synchronous reluctance motors," in *2012 XXth International Conference on Electrical Machines*, pp. IEEE, 2012, 994–1000.

[9] S.-W. Su, C. M. Hackl, and R. Kennel, "Analytical prototype functions for flux linkage approximation in synchronous machines," *IEEE Open Journal of the Industrial Electronics Society*, vol. 3, pp. 265–282, 2022.

[10] K. Corzine, B. T. Kuhn, S. Sudhoff, and H. Hegner, "An improved method for incorporating magnetic saturation in the qd synchronous machine model," *IEEE Transactions on Energy Conversion*, vol. 13, no. 3, pp. 270–275, 1998.

[11] C. Perez-Rojas, "Fitting saturation and hysteresis via arctangent functions," *IEEE Power Engineering Review*, vol. 20, no. 11, pp. 55–57, 2000.

[12] E. Armando, P. Guglielmi, G. Pellegrino, M. Pastorelli, and A. Vagati, "Accurate modeling and performance analysis of IPM-PMASR motors," *IEEE Transactions on Industry Applications*, vol. 45, no. 1, pp. 123–130, 2009.

[13] H. A. A. Awan, Z. Song, S. E. Saarakkala, and M. Hinkkanen, "Optimal

torque control of saturated synchronous motors: Plug-and-play method," *IEEE Transactions on Industry Applications*, vol. 54, no. 6, pp. 6110–6120, 2018.

[14] S. Li, D. Han, and B. Sarlioglu, "Modeling of interior permanent magnet machine considering saturation, cross coupling, spatial harmonics, and temperature effects," *IEEE Transactions on Transportation Electrification*, vol. 3, no. 3, pp. 682–693, 2017.

[15] S. Ferrari and G. Pellegrino, "SyR-e: synchronous reluctance evolution," *Available online: https://github.com/SyR-e/syre_public*, (accessed October 2023).

Francesco Lelli (Student Member, IEEE) received the B.S. degree in computer and system engineering and the M.S. degree in control engineering respectively in 2018 and 2021 from Sapienza - University of Rome, Rome, Italy. Since 2021 he is a PhD student with the Department of Astronautical, Electrical and Energy Engineering. Between 2023 and 2024 he was a Visiting Student with the School of Electrical Engineering, Aalto University, Espoo, Finland. His research focuses on permanent magnet motor drives.

Mr. Lelli is currently a Student Member of the IEEE Industry Applications Society and IEEE Power Electronics Society.

Marko Hinkkanen (Fellow, IEEE) received the M.Sc.(Eng.) and D.Sc.(Tech.) degrees in electrical engineering from the Helsinki University of Technology, Espoo, Finland, in 2000 and 2004, respectively. He is currently an Associate Professor (tenured) with the School of Electrical Engineering, Aalto University, Espoo, Finland. His research interests include electric machine drives, power converters, and control systems.

Dr. Hinkkanen has received eight paper awards, including the 2016 ICEM Brian J. Chalmers Best Paper Award. He was the corecipient of the 2020 SEMIKRON Innovation Award. He is an Associate Editor of IEEE Transactions on Energy Conversion and the IET Electric Power Applications.

Fabio Giulii Capponi (Member, IEEE) received the M.S. and Ph.D. degrees in electrical engineering from the University of Rome "La Sapienza", Rome, Italy, in 1994 and 1998, respectively. He has been with the University of Rome "La Sapienza" since 1996. Since 2020, he has been a Full Professor with the Department of Astronautical, Electrical and Energy Engineering. In 2003 and 2004, he was a visiting scholar with the Wisconsin Electrical Machines and Power Electronics Consortium, University of Wisconsin, Madison, WI, USA. He is an author or co-Author of more than 90 published technical papers. His current research interests include permanent magnet motor drives and multi-physics design of electrical machines.

Prof. Giulii Capponi is a registered professional engineer in Italy and is member of the IEEE Industry Applications, the IEEE Industrial Electronics and the IEEE Power Electronics societies. He is a member of the IEEE IAS Industrial Drives Committee, the Electric Machines Committee, and the Transportation Systems Committee. He was the recipient of the 2014 First Prize Paper Award and the 2016 Third Prize Paper Award, both from the IAS Industrial Drives Committee.